CrossMark

Research Paper

One step hydrothermal synthesis of TiO₂ with variable HCl concentration: Detailed characterization and photocatalytic activity in propene oxidation

L. Cano-Casanova, A. Amorós-Pérez, M. Ouzzine[1], M.A. Lillo-Ródenas*, M.C. Román-Martínez

MCMA Group, Department of Inorganic Chemistry and Materials Institute, Faculty of Sciences, University of Alicante, Ap.99, E-03080 Alicante, Spain

A B S T R A C T

TiO₂ materials have been prepared by a novel one-step hydrothermal synthesis method at mild conditions (low temperature and time) using titanium tetraisopropoxide as precursor and HCl solutions of different concentration, ranging from 0.5 to 12 M. A detailed physico-chemical characterization has been done, putting especial attention to the quantification of crystallinity and surface OH content. All the obtained samples have high surface areas (100–135 m²/g), small anatase crystal size (8–11 nm) and high crystallinity (around 80%). The concentration of the HCl used in the synthesis has a significant effect on the two first mentioned parameters and on the proportion of crystalline phases (anatase-brookite-rutile) developed. There is a good correlation between the amount of hydroxyl surface groups and the specific surface area (S_{BET}), but regarding surface density of OH groups there are, as well, some differences between samples (the samples with higher OH surface densities are those prepared with less concentrated HCl solutions).

Most of the prepared photocatalysts are more active than commercial TiO₂-P25 in the gas phase oxidation of propene at low concentration. The best photocatalytic performance is found for samples prepared with 0.5 and 0.8 M HCl, what can be explained by a suitable combination of properties: high surface area and developed porosity, high surface OH groups' content and density and large proportion of anatase with small crystal size.

1. Introduction

TiO₂ materials have appealed considerable interest as photocatalysts for many applications, among which the decomposition of harmful organic pollutants can be pointed out [1–3]. TiO₂ photocatalysts show outstanding properties like excellent oxidative capability, chemical stability, low price, non-toxicity and biocompatibility [4–6]. For this reason, an intense research is being devoted to develop simple and suitable synthesis methods to obtain TiO₂ with improved photocatalytic efficiency, and to broaden the knowledge of how the physical and chemical properties of TiO₂ determine its photocatalytic activity [7–11].

It is known that the reagents and conditions used in the TiO₂ synthesis strongly determine the key physical and chemical properties of the photocatalysts. In particular, the main properties relevant to the catalytic performance are: surface area, crystalline structure and crystalline phases present, surface chemistry and optical behavior [12–15].

It is usually accepted that the larger the surface area, the higher the catalytic activity, in accordance with the superficial reactions involved in the photocatalytic process [16]. However, in materials like TiO₂, the surface area is strongly linked with the degree of crystallinity and crystal size and, in general, large surface areas correspond to materials with relatively low crystallinity and/or small crystal size [16]. Therefore, because these two properties of TiO₂ (large surface area and amorphous contribution) have, in principle, opposite effects in the photocatalytic performance, a proper balance of them should be considered as the most suitable situation.

Together with the degree of crystallinity, the presence of different crystalline phases is a crucial and controversial parameter that affects the photocatalytic performance of TiO₂ in different applications. On one hand, crystalline TiO₂ seems to be more effective than amorphous titania to prevent recombination of electrons (e⁻) and holes (h⁺) [17]. Maybe because of that, most references just deal with the characterization of crystalline TiO₂, setting aside the analysis of the amorphous contribution, leaving unregarded the degree of crystallinity and the fact that amorphous titania could have some positive influence [17–22]. On the other hand, while in some works anatase is considered as the most photoactive TiO₂ crystalline phase [23–25], other published papers state that materials containing different TiO₂ polymorphs (mainly anatase with some rutile) are more active in oxidation processes

---

[26–29]. This synergistic positive effect of mixed phases has been attributed to a lower electron-hole recombination rate [30,31], and/or to particular defects in the rutile/anatase interface in which charge transfer complexes would be favorable [32].

Although brookite is frequently encountered as a by-product in TiO_2 photocatalysts prepared by sol-gel or hydrothermal methods [33], it is less studied than anatase and rutile. In general, data about pure brookite are lacking mainly because of the difficulty of synthesizing this metastable phase with a high purity, being brookite the least known TiO_2 photocatalyst [34]. In recent years, several studies have dealt with the behavior of brookite in photocatalytic oxidation applications [34,35], but its role has not been clearly stated yet.

Surface chemistry of TiO_2 has received much less attention than its crystallinity. Some studies report that surface −OH groups play an important role in the activity [36,37], acting as capture centers for the photoexcited electrons [38] and preventing recombination of electrons and holes [18,39]. It has also been published that adsorbed water and hydroxyl groups can react with generated holes to produce hydroxyl radicals [30], which are powerful oxidants in the degradation of organic compounds [37]. The OH concentration depends on the surface area, but it also seems to be related with the TiO_2 phases and degree of crystallinity [28,40]. In contrast with what happens with other parameters, there is not a widely accepted standard method to characterize and quantify the surface chemistry of TiO_2.

As mentioned above, the preparation procedure strongly determines the TiO_2 physical and chemical properties, but it must be noted that the available methods have different degrees of complexity and cost. The sol-gel synthesis is widely employed due to the inexpensive equipment required, the low temperatures used and the high homogeneity and purity of the obtained product [41–46]. In contrast, hydrothermal (HT) techniques have been much less used. They are recently becoming interesting tools for advanced nanomaterials' synthesis and potential methods for preparing highly crystalline TiO_2 [12,47,48]. However, they are more complex because two steps and the use of surfactants and co-surfactants [49–51] or organic solvents, like *n*-hexane or cyclohexane [50–52], are usually involved.

In both methods, the nature and concentration of the acid hydrolysis medium used seem to play a substantial role in controlling the morphology and crystal structure of the synthesized TiO_2 [26,49–62]. Nitric, sulfuric, acetic or hydrochloric acids have been used [52,61,62], and it has been found that not only the acid concentration, but also the nature of the anion counterpart affects the nucleation process, the crystal growth and the morphology of TiO_2. It has been reported that SO_4^{2-} and CH_3COO^- anions could retard the formation of rutile [52,61], whereas this phase is easily formed in HNO_3 or HCl media [52,61,62]. Besides, the presence of Cl^- anions seems to lead to smaller TiO_2 crystals [61] and the use of hydrochloric acid has the advantage of its lower price.

In this context, the present study focuses on the synthesis of TiO_2 photocatalysts by a one-step hydrothermal process at low temperature and short time using aqueous HCl solutions as hydrolysis media. The investigated variable is the concentration of the HCl solution. Special attention has been paid to the characterization of the prepared materials, particularly because properties like the degree of crystallinity and the surface chemistry are not considered in many studies; and aspects like the detailed distribution of crystalline phases and their role in photocatalysis are sometimes controversial.

The catalysts have been tested in the gas phase photocatalytic oxidation of propene at low concentration, 100 ppmv, trying not only to develop effective photocatalysts for this reaction, but also to determine the role of the TiO_2 properties on their catalytic performance. Propene has been selected as a representative substance of VOCs (Volatile Organic Compounds). It is present in vehicle emissions, in many industrial effluents, such as those of petrochemical plants, foundry operations and others [63,64], and it is also an important component of tobacco smoke [65,66]. The test is carried out at low propene

concentration because this is usually the case for VOCs in gas effluents and the implementation of efficient removal techniques is difficult and costly in these conditions [67].

2. Experimental

2.1. Materials

Titanium (IV) tetraisopropoxide (TTIP, 97%) was purchased from Sigma-Aldrich. Absolute ethanol (C_2H_6O, 99.8%) and hydrochloric acid (HCl, 37%) were supplied by Panreac. All reactants have been used without further purification. A commercial TiO_2 material, P25 from Evonik (previously Degussa), has been used as reference photocatalyst.

2.2. Preparation of TiO_2 materials

TiO_2 was prepared by hydrothermal synthesis using a procedure adapted from the sol-gel method described by Wang et al. [56]. In a typical synthesis, 4 ml TTIP and 20 ml ethanol were stirred at room temperature for 1 h, and then a mixture of HCl solution (4 ml of 0.5, 0.8, 1, 3, 5, 7 or 12 M concentration) and ethanol (10 ml) was added dropwise. The mixture was continuously stirred for 1 h, and then it was transferred to a 50 ml Teflon-lined stainless steel autoclave, which was heated in an oven at 180 °C for 12 h and then cooled down to room temperature. Afterwards, the solid was filtered, dried at 100 °C for 12 h and, finally, heat treated in air in a muffle at 5 °C/min up to 350 °C, for 2 h.

The synthesized materials are named TiO_2-xM, where x refers to the molar concentration of the HCl solution used. Note that the acid concentration in the synthesis pot is about 10 times lower (i.e. if 4 ml of 12 M HCl solution are used, considering that the total volume is 38 ml, the HCl concentration in the synthesis medium is 1.27 M). [HCl] has been used as an abbreviation of HCl solution concentration in some parts of the manuscript.

2.3. Characterization

Porous texture was characterized by N_2 adsorption at −196 °C in a volumetric Autosorb-6 B apparatus from Quantachrome. The samples were previously degassed at 250 °C for 4 h. The BET equation was applied to the nitrogen adsorption isotherms to get the apparent BET surface areas (S_{BET}). The Dubinin–Radushkevich equation was applied to the N_2 adsorption data to determine the total micropore volume (V_{DR} N_2, pores with size < 2 nm) [68]. The mesopore volume ($V_{mesopore}$ 2 nm < ø < 50 nm) was calculated as the difference between the volume of N_2 adsorbed at $P/P_0 = 0.9$ and $P/P_0 = 0.2$, expressed as a liquid [69]. The total pore volume (V_T) was determined from the volume of nitrogen adsorbed at a relative pressure of $P/P_0 = 0.99$.

The percentage of crystalline TiO_2, phase composition and crystallite size were determined by X-ray diffraction (XRD) at room temperature. Details on the method used for the determination of the percentage of crystallinity and phase compositions are explained in the XRD results section. The XRD patterns were recorded both for TiO_2 samples and for mixtures of these samples and CaF_2 (50%, w/w), using the equipment Miniflex II Rigaku (30 kV/15 mA) with Cu Kα radiation and a scanning rate of 2°/min, in the 2θ range 6–80°. The average crystallite size, referred to as crystal size, was calculated by the Scherrer equation (Eq. (1)) [70]:

$$B = \frac{K\lambda}{\beta cos\theta} \tag{1}$$

where B is the average crystallite size (nm); λ is the wavelength of the radiation used (0.1540 nm for Cu Kα), K is the Scherrer constant (K = 0.93) [70], β is the full width at half maximum intensity (FWHM) and θ is the angle associated to the main peak of the studied phase (these peaks are those at 2θ values of 25.3, 27.5 and 30.8° for anatase, rutile and brookite, respectively).

The materials' morphology was studied by scanning electron microscopy in a JEOL JSM-840 instrument.

The surface chemistry of the TiO_2 materials was analyzed by: i) Fourier transform infrared (FTIR) spectroscopy (FTIR JASCO 4100) in transmission mode from 400 to 4000 cm^{-1}, and ii) by thermogravimetry (TG SDT Q600) in N_2 flow (50 ml/min), with a three steps temperature program: 10 °C/min up to 120 °C, 15 min isothermal at 120 °C, and 10 °C/min from 120 to 750 °C.

The optical absorption properties were studied by UV–vis/DR spectroscopy (Jasco V-670, with integrating sphere accessory and powder sample holder). $BaSO_4$ was used as the reference standard and the reflectance signal was calibrated with a Spectralon standard (Labsphere SRS-99-010, 99% reflectance).

The absorption edge wavelength was estimated from the intercept at zero absorbance of the high slope portion of each individual spectrum in the range 200–800 nm (absorbance method). Then, the band gap can be calculated [71] as:

$$Eg = \frac{1239.8}{\lambda} \qquad (2)$$

where Eg is the band gap energy (eV) and λ is the edge wavelength (nm).

Indeed, indirect and direct electron transitions were also supposed and calculation of the band gaps was performed by plotting $(F(R)h\nu)^{1/2}$ vs $h\nu$ (indirect method) and $(F(R)h\nu)^2$ vs $h\nu$ (direct method), according to reference [72].

2.4. Photocatalytic oxidation of propene

The experimental system used to perform the activity tests was designed in our laboratory and basically consists of a quartz reactor (AFORA) and a 365 nm Philips UV lamp (UV-A) placed parallel to the quartz reactor at a distance of about 1 cm. The assembly quartz reactor-lamp is surrounded by a cylinder covered by tinfoil. A scheme of this system is shown elsewhere [73].

In a typical experiment, 0.11 g photocatalyst were placed on a quartz wool plug inside the reactor and then, after purging with helium, a stream of 100 ppmv propene in air (30 or 60 ml/min (STP)) was passed through the reactor at 25 °C, being the outlet gas continuously analyzed by mass spectrometry (Balzers, Thermostar GSD 301 01). Once the propene concentration is stable (after about 3 h) the lamp is switched on and kept working until a stationary propene signal is achieved (usually 3 h).

The experiments were repeated at least twice to check reproducibility. Propene conversion was calculated using the following expression:

$$Propene\ conversion\ (\%) = \frac{C_{initialC3H6} - C_{stationaryC3H6}}{C_{initialC3H6}} \times 100 \qquad (3)$$

where $C_{initialC3H6}$ is the initial propene concentration, 100 ppmv, and $C_{stationaryC3H6}$ is the stationary propene concentration reached after a certain time of irradiation.

The carbon dioxide produced during oxidation was followed by mass spectrometry and quantified using a calibrated cylinder (300 ppmv CO_2 in helium). Water evolution was also followed by this technique and a mass scan was carried out to determine if additional oxidation compounds were present in the outlet stream.

3. Results and discussion

3.1. Characterization of TiO_2 samples

3.1.1. Textural properties

Fig. 1 shows the N_2 adsorption-desorption isotherms of the seven TiO_2 samples synthesized using HCl solutions of different concentration. It can be observed that all samples are mesoporous, with type IV
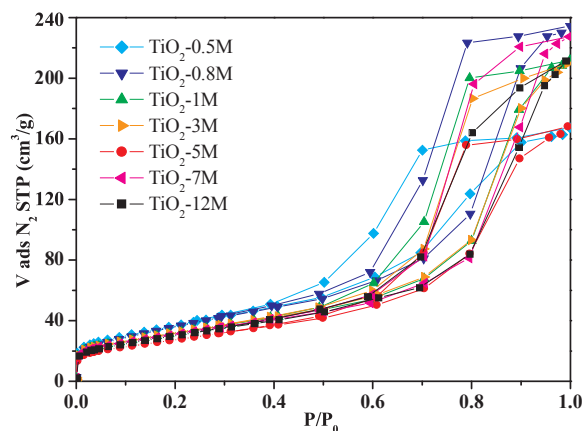

Fig. 1. N_2 adsorption-desorption isotherms at −196 °C of the prepared TiO_2 samples.

adsorption isotherms according to the IUPAC classification [74], but with some significant differences in their porosity.

Table 1 summarizes the textural properties of the synthesized TiO_2 samples and of the TiO_2-P25 reference material. It can be observed that the prepared TiO_2 samples have larger surface areas and pore volumes than the commercial material, and also that the HCl concentration used in the synthesis has a noticeable effect on the textural properties. In general, the surface area decreases as the concentration of the HCl increases. There are clear differences in surface areas and total pore volumes between samples, but the variation of these two parameters is not linked in the same way in all cases. Thus, samples TiO_2-0.5 M and TiO_2-0.8 M have almost the same surface areas, but they differ in their total pore volumes (entries 1 and 2); samples TiO_2–1 M, and TiO_2–3 M (entries 3 and 4), and also samples TiO_2–7 M and TiO_2–12 M (entries 6 and 7), have similar surface areas and similar pore volumes, while samples TiO_2-0.8 M and TiO_2–7 M (entries 2 and 6) have different surface areas and similar pore volumes.

The surface areas and pore volumes shown in Table 1 are three to four times higher than those of other reported TiO_2 materials also prepared by hydrothermal synthesis using HCl [52,60], with the added advantage of eluding the use of *n*-hexane [52] or of a two-step-procedure [60]. In some works, porosity characterization of the synthesized TiO_2 is not presented; this is the case, for example, of the two-step HCl-assisted hydrothermal process based on cetyl trimethylammonium bromide [49] and of the microemulsion method reported by Wu et al. [51].

3.1.2. XRD analysis

Fig. 2 shows the XRD patterns obtained for the synthesized TiO_2 samples. The characteristic peaks of anatase appear at 2θ values of 25.3° (101), 37.8° (004), 48.0° (200), 54.5° (105), 55.0° (211), 62.7° (204), 70.4° (116) and 74.5° (220), those of brookite appear at 2θ values 25.3° (120), 25.7° (111) and 30.8° (121) [70], whereas the peaks located at 27.5° (110), 36.1° (101) and 54.4° (211) correspond to rutile [75]. It must be mentioned that the main diffraction peak of anatase (101) overlaps with the (120) and (111) peaks of brookite [70].

Taking into account this information, data of Fig. 2 show that samples TiO_2–0.5 M and TiO_2–12 M contain anatase and brookite, whereas samples TiO_2–0.8 M, TiO_2–1 M, TiO_2–3 M, TiO_2–5 M and TiO_2–7 M contain anatase, brookite and rutile in different proportions. That is, the three TiO_2 crystalline phases are present in most samples, and rutile is only absent in those prepared with the lowest and highest HCl concentrations.

The phase composition (in wt.%) of crystalline TiO_2 can be calculated from the integrated areas of the main peaks of anatase (101), brookite (121) and rutile (110) by means of the following expressions [70]:

Table 1

Textural properties for the TiO$_2$ materials synthesized using HCl solutions of different concentration and for the TiO$_2$-P25 reference material.

Entry	Sample	[HCl]* (M)	S$_{BET}$ (m^2/g)	V$_{DR}$ N$_2$ (cm^3/g)	V$_{mesopore}$ (cm^3/g)	V$_T$ (cm^3/g)
1	TiO$_2$–0.5M	0.05	135	0.05	0.20	0.26
2	TiO$_2$–0.8M	0.08	134	0.05	0.29	0.36
3	TiO$_2$–1M	0.11	116	0.04	0.25	0.33
4	TiO$_2$–3M	0.32	117	0.04	0.25	0.32
5	TiO$_2$–5M	0.53	100	0.04	0.20	0.26
6	TiO$_2$–7M	0.74	113	0.04	0.28	0.35
7	TiO$_2$–12M	1.27	110	0.04	0.26	0.32
8	TiO$_2$–P25	–	55	0.02	0.07	0.18

*HCl concentration in the synthesis solution as a result of the mixture of 4 ml TTIP, 30 ml ethanol and 4 ml HCl of the concentration indicated in the samples' nomenclature.

$$W_A\% = \frac{K_A I_A}{K_A I_A + I_R + K_B I_B} \qquad (4)$$

$$W_B\% = \frac{K_B I_B}{K_A I_A + I_R + K_B I_B} \qquad (5)$$

$$W_R\% = \frac{I_R}{K_A I_A + I_R + K_B I_B} \qquad (6)$$

Where W_A, W_B and W_R are the weight fractions of anatase, brookite and rutile, respectively, and $I_{A(101)}$, $I_{B(121)}$ and $I_{R(110)}$ are the integrated intensities of the (101) anatase, (121) brookite and (110) rutile peaks in the XRD spectra, respectively. K_A and K_B are correction coefficients optimized by Gribb and Banfield [76], and Zhang and Banfield [70], with $K_A = 0.886$ and $K_B = 2.721$ values.

If the sample only contains anatase and rutile, as it is the case in P25, the weight fraction of rutile (W_R) can be calculated from [70]:

$$W_R\% = \frac{I_R}{0.884 I_A + I_R} \cdot 100 \qquad (7)$$

Overlapping of the main diffraction peak of anatase (101) with the (120) and (111) brookite peaks confers some complexity to the analysis. A numerical deconvolution of the peak located at about 25° was carried out to determine the areas of (120) and (111) brookite peaks. The procedure for such deconvolution is briefly described next. As indicated above, the XRD pattern in the 22–34° 2θ range comprises peaks corresponding to the following crystal faces: anatase (101) (at 25.3°, 100% intensity, ref. JCPDS No. 21–1272), rutile (110) (at 27.5°, 100% intensity, ref. JCPDS No. 21–1276) and brookite (120), (111) and (121) (at 25.3°, 25.7° and 30.8°, 100%, 80% and 90% intensity, respectively, ref. JCPDS No. 29–1360) [70]. After baseline subtraction, and taking into account the peak positions and intensities, this fragment of the XRD spectra was fitted by 50%-50% Lorentzian-Gaussian curves. Fig. 3 shows, as an example, the deconvolution performed in the XRD pattern of sample TiO$_2$–3 M. For the fitting, it is assumed that broadening of
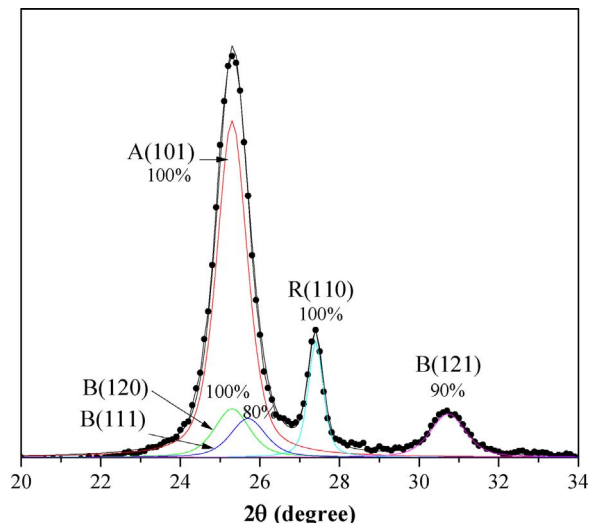

Fig. 3. Deconvolution of XRD patterns of sample TiO$_2$–3 M. Points correspond to experimental data.

(120), (111) and (121) brookite peaks is the same, and the exponents of the Lorentzian-Gaussian curves for the brookite peaks are set equal as well.

Thus, $I_{A(101)}$ was calculated by subtracting the area of B(111) and B(120) peaks from the A(101) area (Fig. 3). The weight fractions of anatase, brookite and rutile (W_A, W_B and W_R) in crystalline TiO$_2$ were calculated according to Eqs. (4)–(6) and are presented in Table 2.

Data in Table 2 shows that the concentration of the HCl solution used in the TiO$_2$ synthesis has an important influence on the phase composition of the prepared samples.

Average crystal size, calculated from FWHM values of the corresponding peaks previously deconvoluted, has been also included in
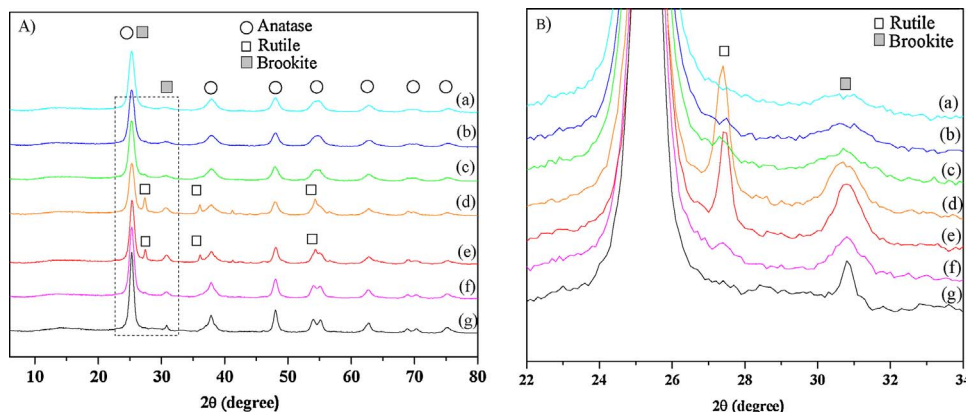

Fig. 2. A) XRD patterns of TiO$_2$ samples prepared using HCl solutions of different concentration: (a) TiO$_2$-0.5 M, (b) TiO$_2$–0.8 M, (c) TiO$_2$–1 M, (d) TiO$_2$–3 M, (e) TiO$_2$–5 M, (f) TiO$_2$–7 M and (g) TiO$_2$–12 M. B) Amplified 22–34° 2θ range of Fig. 2A.

Table 2
Weight fractions of anatase, brookite and rutile in the crystalline phase of TiO$_2$ samples and average crystallite sizes.

Sample	Weight fraction			Average crystallite size (nm)		
	W_A (%)	W_B (%)	W_R (%)	A	B	R
TiO$_2$–0.5M	86	14	–	8	5	–
TiO$_2$–0.8M	80	19	1	8	6	17
TiO$_2$–1M	78	20	2	9	6	17
TiO$_2$–3M	61	27	12	9	8	20
TiO$_2$–5M	66	27	7	10	9	23
TiO$_2$–7M	83	16	1	10	10	24
TiO$_2$–12M	88	12	–	11	17	–
TiO$_2$–P25	84	–	16	22	–	28–>

A = Anatase, B = Brookite and R = Rutile.

Table 3
Crystalline properties of TiO$_2$ samples determined from XRD patterns.

Sample	Crystalline contribution			Amorphous Contribution (%)
	A_{Cryst} (%)	B_{Cryst} (%)	R_{Cryst} (%)	
TiO$_2$0.5M	69	11	–	20
TiO$_2$0.8M	60	16	1	23
TiO$_2$–1M	62	17	2	19
TiO$_2$–3M	45	23	11	21
TiO$_2$–5M	50	23	6	21
TiO$_2$–7M	64	14	1	21
TiO$_2$–12M	66	9	–	25
TiO$_2$–P25	73	–	14	13

A = Anatase, B = Brookite and R = Rutile.

Table 2. It can be observed that the crystal size increases with the concentration of the HCl solution used in the synthesis.

The next target was to quantify the crystalline and amorphous TiO$_2$ in each sample, being the latter a relevant parameter that has not been considered in most studies. In the procedure reported by Jensen et al. [22], TiO$_2$ crystallinity is determined with respect to a 100% crystalline CaF$_2$ sample using XRD spectra of 50/50 (w/w) TiO$_2$/CaF$_2$ mixtures. The authors indicate that the amount of crystalline anatase (A$_{cryst}$) and rutile (R$_{cryst}$) can be calculated using these equations:

$$A_{Cryst} = \frac{\frac{A_{Anatase,101}}{A_{CaF2,220}} \times 100}{1.25} \tag{8}$$

$$R_{Cryst} = \frac{\frac{A_{Rutile,110}}{A_{CaF2,220}} \times 100}{0.90} \tag{9}$$

Where A$_{Anatase,101}$, A$_{Rutile,110}$ and A$_{CaF2,220}$ are the areas determined from the TiO$_2$/CaF$_2$ XRD pattern, and 1.25 and 0.9 are, respectively, the ratio between areas of the same peaks when a pure anatase or rutile crystalline TiO$_2$ sample is used.

However, the procedure does not include a similar calculation for brookite, and we have not found in the literature a value for the area ratio of the (121) peak of pure 100% crystalline brookite to the pure 100% crystalline CaF$_2$ (220) peak, necessary to complete the assessment of crystalline TiO$_2$ in this way. The study of Bellardita et al. [77] only focuses on brookite and uses this equation:

$$\frac{FWHM_{CaF2,111}}{FWHM_{Brookite,121}} = 1.04 \tag{10}$$

in which FWHM values are considered, instead of areas.

Calculation of brookite content in our samples with the equation of Bellardita et al. [77] did not provide coherent data that agree with our experimental XRD patterns and with the brookite weight fractions shown in Table 2. Because of that, in the present work we propose and use a new method to have the complete quantification of crystalline TiO$_2$ in samples that contain anatase, brookite and rutile. After calculating crystalline anatase (A$_{Cryst}$) and rutile (R$_{Cryst}$) by Eqs. (8) and (9), we determine crystalline brookite with a procedure based on the following idea: the ratio between the amount of two crystalline phases should be equal to the analogous ratio between the weight fractions. Thus, to determine B$_{Cryst}$ we assume B$_{Cryst}$/A$_{Cryst}$ = W$_B$/W$_A$ and B$_{Cryst}$/R$_{Cryst}$ = W$_B$/W$_R$ (W$_A$, W$_B$ and W$_R$ were previously calculated by Eqs. (4)–(6), Table 2), what leads to two values of B$_{cryst}$ calculated as follows:

$$B_{Cryst}1 = \frac{W_B}{W_A} \times A_{Cryst} \tag{11}$$

$$B_{Cryst}2 = \frac{W_B}{W_R} \times R_{Cryst} \tag{12}$$

Taking into account that B$_{Cryst}$ 1 and B$_{Cryst}$ 2 should be similar for the validity of the procedure, the arithmetic media between these two values has been taken as the actual B$_{Cryst}$. The values of A$_{Cryst}$, R$_{Cryst}$ and B$_{Cryst}$ are included in Table 3.

The B$_{Cryst}$ data obtained using the procedure previously commented have allowed us to determine a value for the area ratio between 100% crystalline brookite and CaF$_2$, as done by Jensen et al. for anatase and rutile. Thus, Eq. (13) is analogous to Eqs. (8) and (9) corresponding to anatase and rutile:

$$B_{Cryst} = \frac{\frac{A_{Brookite,121}}{A_{CaF2,220}} \times 100}{X} \tag{13}$$

where B$_{Cryst}$ is the arithmetic media of the values calculated from Eqs. (11) and (12), A$_{Brookite,121}$ and A$_{CaF2,220}$ are the areas determined from the TiO$_2$/CaF$_2$ XRD pattern of the TiO$_2$/CaF$_2$ (50/50, (w/w)) mixture and, thus X is the area ratio between 100% crystalline brookite and CaF$_2$. The results of the present study have allowed to determine the value of X = 0.37.

This value, 0.37, can be used to determine the crystalline brookite by the procedure proposed by Jensen et al. [22].

The percentage of crystalline (W$_{Cryst}$) and amorphous (W$_{Am}$) phases present in the TiO$_2$ samples was finally determined as:

$$W_{Cryst} = A_{Cryst} + R_{Cryst} + B_{Cryst} \tag{14}$$
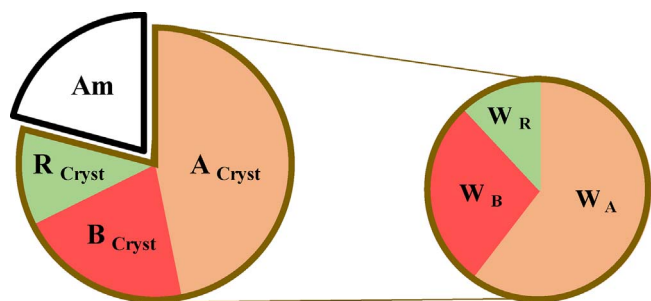
$$W_{Am} = 100 - W_{Cryst} \tag{15}$$

A$_{Cryst}$ and R$_{Cryst}$ were calculated by using Jensen's method and B$_{Cryst}$ was calculated as indicated above.

The calculated parameters are presented in Table 3, where the data obtained for the reference TiO$_2$-P25 have also been included. Note that the amorphous phase determined for P25 by this method is similar to the values reported in the literature [21,22,78,79].

Scheme 1 shows, for clarity purposes, a graphical explanation of the crystalline/amorphous fraction and the crystalline phase distribution.

According to data of Table 3, the prepared TiO$_2$ samples show a high crystallinity (~80%). However, compared with TiO$_2$-P25, the prepared samples contain a higher amorphous phase fraction, what is consistent with the higher surface area of these materials (100–135 vs 55 m^2/g).

The variation of the phase compositions with the concentration of the HCl solution used in the synthesis can be better appreciated in Fig. 4. This figure shows that the percentage of anatase decreases with the HCl concentration increase up to 3 M, and then it increases for higher [HCl]. In contrast, the percentage of brookite and rutile vary in an opposite way, whereas the percentage of crystalline phases, and hence the amorphous phase content, is similar in all the samples. Thus, as the HCl concentration increases, the phase composition of the samples changes in the following way: A–B→A–B–R→A–B.

Scheme 1. Graphical explanation of the crystalline/amorphous fraction and the crystalline phase distribution (for the meaning of depicted parameters see the text). Brown line: Crystalline TiO_2, Black line: Amorphous TiO_2.
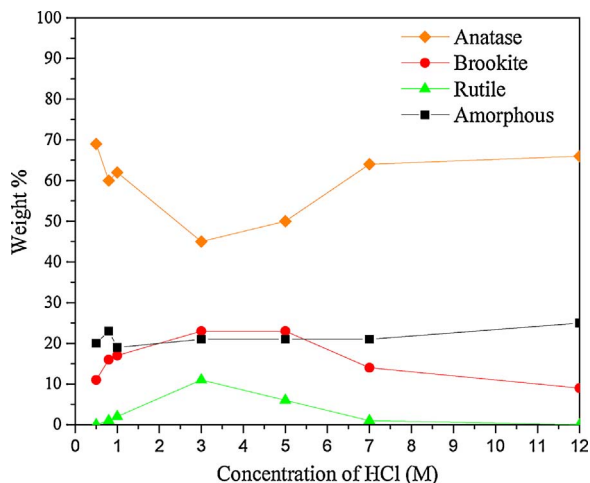

Fig. 4. Weight percentage of crystalline (anatase, brookite and rutile) and amorphous phases in the TiO_2 samples as a function of HCl concentration used in the synthesis.

This variation in the composition of the crystalline phase with the concentration of the HCl used in the synthesis has some similarities with the results reported by Dai et al. [49]. These authors prepared TiO_2 by a two-step hydrothermal method in which a hexagonal structured nanocrystalline titania (cetyltrimethylammonium bromide) nanoskeleton was further treated with HCl solution (from 0.1 to 8 M). Using their lower and higher [HCl], the samples contained only anatase, whereas after treatment with HCl of intermediate concentration rutile was also formed.

The formation of different TiO_2 phases must be determined by the mechanisms of *in-situ* transformation and dissolution and recrystallization that prevail at different HCl concentrations [49].

The formation of brookite is likely related to the relatively low activation energy for the transformation of anatase to brookite (11.9 kJ/mol), what allows such a transformation to proceed at low temperature [70]. Temperature conditions of the present work (180 °C in the hydrothermal synthesis, and 350 °C in the heat treatment) seem to favour the development of brookite and to hinder the extensive transformation of anatase and brookite to rutile. Furthermore, as reported in the literature, the interface B-A provides potential nucleation sites for the A → R transition [80]. Therefore, samples with a higher brookite content are prone to suffer the A–R transition, in agreement with the results presented in Table 3.

The influence of the HCl concentration on the TiO_2 synthesis is reported in a limited number of references [49–51,60]. However, because of the important differences in the experimental conditions used, it is often difficult to compare results. In any case, it can be concluded that the concentration of the hydrochloric acid plays an important role in the development of the crystalline structure of TiO_2, but the samples' properties noticeably differ depending on the synthesis method and the
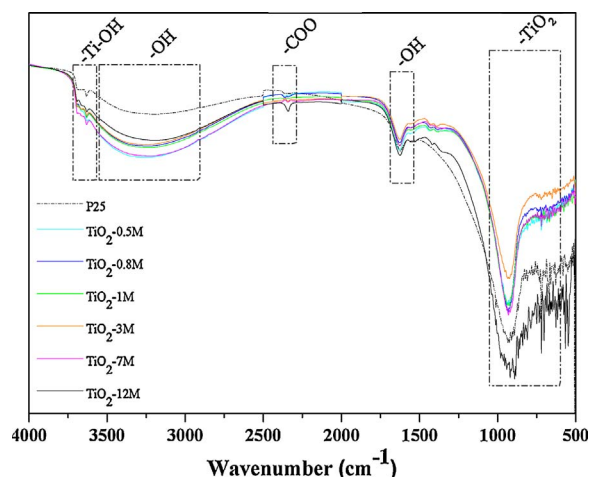

Fig. 5. FTIR spectra of TiO_2 samples prepared with HCl solutions of different concentration and of TiO_2-P25 reference material.

experimental conditions selected.

3.1.3. Scanning electron microscopy characterization

SEM images (Supplementary information, Fig. S1) show that all the samples, with the exception of TiO_2–12 M, present an irregular morphology. The grains of sample TiO_2–12 M have spherical shape and this seems to indicate that a HCl concentration above a certain minimum value is required for the development of such morphology [33,52].

3.1.4. Surface chemistry characterization

The TiO_2 surface chemistry has been scarcely investigated, probably because of the difficulty in the characterization and quantification of surface species. In this work, we have approached such a study by FT-IR and TG.

The obtained FTIR spectra (Fig. 5) show the following main patterns: i) The broad band at about 3350–3450 cm^{-1} is attributed to the O−H stretching of water physisorbed on the TiO_2 surfaces and hydrogen-bonded hydroxyl groups [81]. ii) Bands at 3600–3700 cm^{-1} are assigned to OH groups bound to single Ti atoms [82]; peaks at 3693 and 3632 cm^{-1} correspond to the stretching modes of free −OH groups on anatase Ti^{4+}, while the band at 3665 cm^{-1} can be assigned to bridging hydroxyls [82,83]. There is no evidence of Ti^{3+}−OH bands (that would have appeared at 3617 cm^{-1} [84]). iii) The band near 2300 cm^{-1} is due to bidentate carbonate and bicarbonate species [85]. iv) The band at 1637 cm^{-1} corresponds to the O−H bending modes of water molecules [81]. v) The strong absorption observed below 850 cm^{-1} is attributed to lattice vibrations of TiO_2 [81].

Comparison between FTIR data of the different samples shows that the band at 1637 cm^{-1} (-OH bending modes of water) is similar for all the samples, and no significant differences between samples are observed in the 3600–3700 cm^{-1} region. However, the band at about 3350–3450 cm^{-1} (physisorbed water molecules) is more intense in the TiO_2 samples than in the P25 reference material. We can postulate that this difference arises from the larger surface areas of the TiO_2 prepared samples, which leads to larger content of physisorbed water molecules.

The IR band due to the TiO_2 lattice vibrations (at 850 cm^{-1}) is similar for TiO_2-0.5 M, TiO_2-0.8 M, TiO_2–1 M and TiO_2–7 M samples. It is less intense for TiO_2–3 M, likely due to its higher rutile content, and it is noticeably more intense for TiO_2–12 M, what could be related to its different morphology and larger crystal size.

The presence of COO^- species (band near 2300 cm^{-1}) has only been observed in sample TiO_2–12 M, and such species could be the result of the reaction of HCl with unreacted organic fragments of the TTIP precursor or/and ethanol. The presence of such carbonate groups has been previously reported and attributed to the interaction of Ti-O

Table 4

Humidity, OH type-groups content (in weight percentages), and density of hydroxyl groups (OH_T/S_{BET}).

Sample	Humidity (%)	OH_{weak} (%)	OH_{strong} (%)	OH_{total} (%)	OH_T density x 10^{-18} (OH groups/m^2)
TiO_2–0.5M	1.40	1.48	0.88	2.36	6.19
TiO_2–0.8M	1.26	1.40	0.97	2.37	6.27
TiO_2–1M	1.27	1.34	0.72	2.06	6.29
TiO_2–3M	1.27	1.23	0.69	1.92	5.81
TiO_2–7M	0.94	1.10	0.67	1.77	5.55
TiO_2–12M	1.03	1.12	0.76	1.88	6.05
TiO_2–P25	0.61	0.76	0.51	1.11	10.21

Table 5

Energy band gap (Eg) values obtained from different methods for the prepared TiO_2 samples and for TiO_2-P25 and crystalline phase composition for these samples.

Sample	Eg (eV)[a]	Eg (eV)[b]	Eg(eV)[c]	A-B-R (%)
TiO_2–0.5M	3.06	3.01	3.21	86–14–0
TiO_2–0.8M	2.95	3.04	3.26	80–18–1
TiO_2–1M	2.95	3.03	3.22	78–20–2
TiO_2–3M	2.72	2.87	3.18	61–28–12
TiO_2–5M	2.85	2.89	2.98	66–27–7
TiO_2–7M	2.99	3.02	3.21	83–16–1
TiO_2–12M	3.15	3.14	3.24	88–12–0
TiO_2–P25	2.95	2.96	3.20	84–0–16

[a] absorbance.

[b] indirect allowed transitions.

[c] direct allowed transitions.

bonds with organic molecules present in the reaction medium [86].

Although FTIR gives useful information about the surface chemistry of these materials, a more quantitative approach is necessary to better compare the different samples. For this reason, we have also carried out a TG characterization based on the method reported by Di Paola et al. [21], by which the weight loss in several temperature intervals is assigned to the removal of different surface species: i) 30–120 °C → physically adsorbed water (humidity), ii) 120–300 °C → weakly bonded OH groups and iii) 300–600 °C → strongly bonded OH groups [21].

Table 4 compiles the obtained results. It can be observed that, in general, the samples prepared with the lower concentration HCl solutions show the higher humidity and amount of OH groups, being in all cases higher than in P25.

Analysis of the relationship between OH_T and the specific surface area (S_{BET}) shows a good linearity between both parameters; that is the larger the surface area, the larger the total OH groups content, in agreement with the literature [21,28]. In spite of this, there are some differences in the surface density of total surface hydroxyl groups (calculated as number of OH groups per gram divided by S_{BET} (Table 1) and included in Table 4). The samples with higher OH density are those prepared with less concentrated HCl solutions.

3.1.5. UV–vis analysis of TiO_2

The main problem for the experimental calculation of Eg from optical spectroscopy is based on the adequate selection of the method used for it, considering the possible electronic transitions, which depend on the crystalline phases present in the semiconductor. Some authors have reported that TiO_2 has a direct forbidden gap, which is also degenerated with an indirect allowed transition [87], whereas other authors have reported direct allowed transitions [72]. Because of that, in this work, the band gap energy, Eg, has been calculated by the absorbance method and by plotting $(F(R)h\nu)^{1/2}$ vs $h\nu$ (indirect method) and $(F(R)h\nu)^2$ vs $h\nu$ (direct method) [72], as indicated in the experimental section.

The calculated Eg values are presented in Table 5, where weight fractions of anatase, brookite and rutile in the crystalline phase of TiO_2 (Table 2) have also been included. These data show that the Eg values for the indirect method are in good agreement with those obtained from the absorbance method, while higher Eg values have been obtained
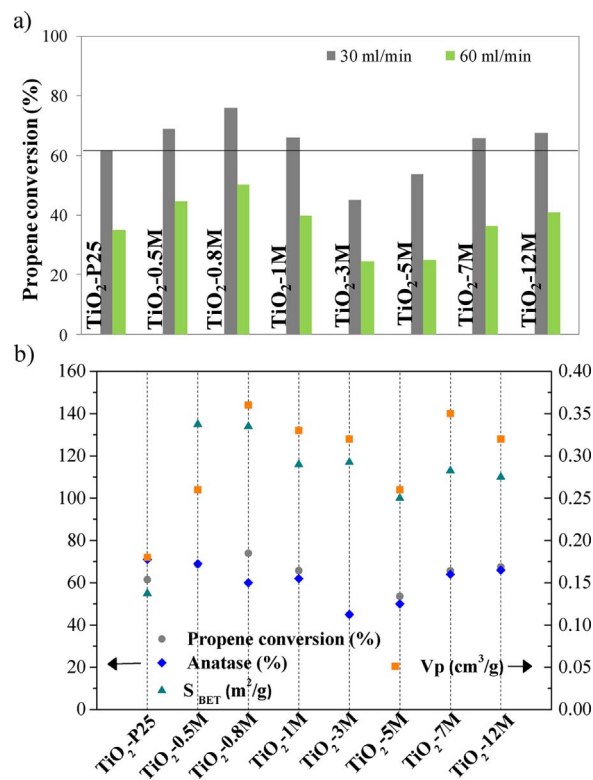

Fig. 6. a) Propene conversion (at 30 and 60 ml/min) for the synthesized TiO_2 samples and for P25 reference, and b) relationship between BET surface area, total pore volume and propene conversion (30 ml/min) in the investigated photocatalysts.
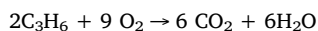
when direct method is used. Since the samples show a mixture of TiO_2 phases, it is difficult to establish the corresponding transition and hence, for simplicity, and considering the good agreement between the tendencies from the three methods, the Eg values obtained from the absorbance method have been used in the discussion.

Data of Table 5 shows that there are significant differences in the Eg values of the prepared samples. As expected, the phase composition strongly affects the band gap, and the obtained data show that the Eg values seem to be directly related with the proportion of anatase in crystalline TiO_2.

3.2. Photocatalytic activity

Fig. 6a shows values of propene conversion obtained with the two flow-rates tested. These results indicate that all the prepared photocatalysts are active, being five of them even more active than the reference P25. Besides, the same tendency is found with the two propene flow-rates, what can be considered as proof of the reproducible behavior of these catalysts. As expected, propene conversion is higher when the lower gas flow is used (because the contact time is longer and/or lower amount of propene molecules have to be oxidized per unit of time).

The mass scan carried out to determine oxidation compounds in the outlet stream reveals that CO_2 is the only oxidation product. Also, quantification of the produced CO_2 has allowed to perform a carbon balance which confirms that total mineralization of propene takes place, according to the following reaction and in agreement with the literature [88,89]:

$$2C_3H_6 + 9\,O_2 \rightarrow 6\,CO_2 + 6H_2O$$

According to Fig. 6a, the activity order of the investigated photocatalysts is the following: TiO_2–0.8 M $\approx$ TiO_2–0.5 M > TiO_2–12 M > TiO_2–1 M > TiO_2–7 M > P25 > TiO_2–5 M > TiO_2–3 M

In order to study the relationship between the photocatalysts' properties and their catalytic activity, propene conversion, BET surface area, pore volume and anatase content of each sample have been plotted in Fig. 6b. A relatively good correlation between the plotted parameters can be observed. However, it must be pointed out that it is extremely difficult to analyse the influence of a particular property of the TiO_2 samples in the catalytic performance because some parameters are closely linked and some of them have opposite effects. For example, the OH content is directly related with the surface area and with the crystalline structure, as mentioned before and as reported in the literature [21,28,40]; However, surface area, total crystallinity and crystal size are related in a complex, almost inverse, way.

A tentative interpretation of the tendencies observed in Fig. 6b is presented next. Samples prepared with 0.8 and 0.5 M HCl show the highest activities, very similar for the two of them. Their superior performance in comparison to the other materials can be explained considering that they contain a large amount of anatase and the highest surface areas. The slightly higher activity of sample TiO_2–0.8 M, despite its lower anatase content, can be attributed to its higher pore volume (see Fig. 6b).

Following the mentioned trend, sample TiO_2–1 M is less active than TiO_2-0.8 M, in agreement with its lower surface area (and less OH groups content) and pore volume. Although the textural parameters of sample TiO_2–3 M are similar to those of TiO_2–1 M, the first one is clearly less active, and this is probably due to its lower anatase content.

As mentioned before, TiO_2–3 M and TiO_2–5 M show the lowest photocatalytic activity. In comparison with the rest of samples, they have the lowest anatase content and the highest amount of rutile and brookite.

Sample TiO_2–5 M is slightly more active than TiO_2–3 M and, thus, it can be assumed that its higher anatase content compensates its poorer textural properties.

In the case of samples TiO_2–7 M and TiO_2–12 M, the balance of properties (higher surface area and pore volume of TiO_2–7 M and higher anatase content in TiO_2–12 M) lead to a slightly higher activity of sample TiO_2–12 M. It can be mentioned that sample TiO_2–12 M has spherical morphology and contains COO^- surface species, but we are not aware about the effect of these characteristics in photoactivity yet.

In summary, the obtained results show that the textural properties of TiO_2 play a relevant role in its catalytic activity. In particular, the specific surface area is a very important parameter because it determines the exposed semiconductor surface and the amount of OH surface groups. The amount of anatase is, as well, a key parameter in the activity of TiO_2 for propene oxidation. This result is in agreement with reported information that assures that the charge carrier recombination rate is lower in anatase than in other crystalline phases [32,90,91]. Anatase is regarded as an indirect semiconductor with phonon assisted electron-hole recombination, what leads to longer life charge carriers [91].

Finally, and taking into account all these results, it can be stated that the activity does not depend separately on any of these parameters, but it is maximized by a convenient combination of them.

4. Conclusions

TiO_2 photocatalysts have been prepared by a one-step simple hydrothermal method. The synthesis is performed in mild conditions (low temperature and time), using HCl solutions of variable concentration as hydrolysis media and avoiding surfactants. The prepared materials have noticeably higher porosity and surface area (100–135 m^2/g) than similar materials prepared by solvothermal method, and also than commercial TiO_2 P25. In general, the surface area of the samples decreases as the concentration of the used HCl increases. Most of the prepared photocatalysts contain anatase, brookite and rutile, in a proportion influenced, as well, by the HCl concentration. The detailed characterization of the crystalline phases has allowed to calculate the amount of each phase and, thus, the crystallinity degree (which is quite high, about 80%) by a methodology proposed in this work.

The surface chemistry has been well characterized; FTIR has revealed some differences between the surface chemistry of the samples, and the amount of surface hydroxyl groups has been determined by TG. The samples with higher surface OH densities are those prepared with less concentrated HCl solutions.

Most of the TiO_2 materials prepared are more active for propene oxidation than the well-known TiO_2–P25 commercial photocatalyst, underlying the interest of the prepared anatase-brookite and anatase-rutile-brookite photocatalysts. A relatively good correlation between propene conversion, BET surface area, pore volume and anatase content has been found. The samples prepared with the less concentrated HCl solutions (TiO_2-0.5 M and TiO_2–0.8 M) show the best photocatalytic performance in this particular application. This means that by selecting the appropriate HCl concentration for the TiO_2 synthesis using the hydrothermal method reported in this work, a suitable combination of properties can be achieved.

Appendix A. Supplementary data

Supplementary data associated with this article can be found, in the online version, at http://dx.doi.org/10.1016/j.apcatb.2017.08.060.

References

[1] H. Yu, K. Zhang, C. Rossi, J. Photochem. Photobiol. A 188 (2007) 65–73.
[2] J. Mo, Y. Zhang, Q. Xu, J.J. Lamson, R. Zhao, Atmos. Environ. 43 (2009) 2229–2246.
[3] L.G. Devi, R. Kavitha, Appl. Catal. B 140-141 (2013) 559–587.
[4] H. Tada, T. Kiyonaga, S. Naya, Chem. Soc. Rev. 38 (2009) 1849–1858.
[5] H. Li, D. Wang, H. Fan, P. Wang, T. Jiang, T. Xie, J. Colloid. Interface Sci. 354 (2011) 175–180.
[6] H. Zhang, G. Du, W. Lu, L. Cheng, X. Zhu, Z. Jiao, Cryst. Eng. Comm. 14 (2012) 3793–3801.
[7] K.R. Reddy, M. Hassan, V.G. Gomes, Appl. Catal. A 489 (2015) 1–16.
[8] L. Wang, Y. Cai, L. Song, W. Nie, Y. Zhou, P. Chen, Colloid Surf. A 461 (2014) 195–201.
[9] M. Danish, S. Ambreen, A. Chauhan, A. Pandey, J. Saudi Chem. Soc. 19 (2015) 557–562.
[10] P. Jiang, W. Xiang, J. Kuang, W. Liu, W. Cao, Solid State Sci. 46 (2015) 27–32.
[11] Y. Wang, Y. He, Q. Lai, M. Fan, J. Environ. Sci. (China) 26 (2014) 2139–2177.
[12] E. Pulido Melián, O. González Díaz, J.M. Doña Rodríguez, G. Colón, J.A. Navío, J. Pérez Peña, Appl. Catal. A 411-412 (2012) 153–159.
[13] B. Wen, C. Liu, Y. Liu, J. Photochem. Photobiol. A 173 (2005) 7–12.
[14] J.C. Yu, J. Yu, L. Zhang, W. Ho, J. Photochem. Photobiol. A 148 (2002) 263–271.
[15] G. Colón, M.C. Hidalgo, G. Munuera, I. Ferino, M.G. Cutrufello, J.A. Navío, Appl. Catal. B 63 (2006) 45–59.
[16] S. Sahni, S.B. Reddy, B.S. Murty, Mater. Sci. Eng. A 452–453 (2007) 758–762.
[17] S.M. Gupta, M. Tripathi, Chin. Sci. Bull. 56 (2011) 1639–1657.
[18] H. Jensen, A. Soloviev, Z. Li, E.G. Søgaard, Appl. Surf. Sci. 246 (2005) 239–249.
[19] B. Ohtani, Y. Ogawa, S.I. Nishimoto, J. Phys. Chem. B 101 (1997) 3746–3752.
[20] G. Benkö, B. Skårman, R. Wallenberg, A. Hagfeldt, V. Sundström, Arkady P. Yartsev, J. Phys. Chem. B 107 (2003) 1370–1375.
[21] A. Di Paola, M. Bellardita, L. Palmisano, Z. Barbieriková, V. Brezová, J. Photochem. Photobiol. A 273 (2014) 59–67.
[22] H. Jensen, K.D. Joensen, J.E. Jørgensen, J.S. Pedersen, E.G. Søgaard, J.

Nanoparticle Res. 6 (2004) 519–526.
[23] C. Hägglund, B. Kasemo, L. Österlund, J. Phys. Chem. B 109 (2005) 10886–10895.
[24] G.M. Zuo, Z.X. Cheng, H. Chen, G.W. Li, T. Miao, J. Hazard. Mater. 128 (2006) 158–163.
[25] X. Wei, G. Zhu, J. Fang, J. Chen, Int. J. Photoenergy 2013 (2013) 1–6.
[26] B.K. Mutuma, G.N. Shao, W.D. Kim, H.T. Kim, J. Colloid. Interface Sci. 442 (2015) 1–7.
[27] C.A. Emilio, M.I. Litter, M. Kunst, M. Bouchard, C. Colbeau-Justin, Langmuir 22 (2006) 3606–3613.
[28] J.T. Carneiro, T.J. Savenije, J.A. Moulijn, G. Mul, J. Phys. Chem. C 115 (2010) 2211–2217.
[29] G. Li, K.A. Gray, Chem. Phys. 339 (2007) 173–187.
[30] R.R. Bacsa, J. Kiwi, Appl. Catal. B 16 (1998) 19–29.
[31] J.M. Warson, A.T. Cooper, J.R.V. Flora, Environ. Eng. Sci. 22 (2005) 666–675.
[32] D.C. Hurum, A.G. Agrios, S.E. Crist, K.A. Gray, T. Rajh, M.C. Thurnauer, J. Electron Spectros. Relat. Phenom. 150 (2006) 155–163.
[33] J.G. Li, T. Ishigaki, X. Sun, J. Phys. Chem. C 111 (2007) 4969–4976.
[34] A. Di Paola, M. Bellardita, L. Palmisano, Catalysts 3 (2013) 36–73.
[35] T.A. Kandiel, A. Feldhoff, L. Robben, R. Dillert, D.W. Bahnemann, Chem. Mater. 22 (2010) 2050–2060.
[36] J. Yu, X. Zhao, J. Du, W. Che, J. Sol-Gel. Sci. Technol. 17 (2000) 163–171.
[37] Z. Ding, G.Q. Lu, P.F. Greenfield, J. Phys. Chem. B 104 (2000) 4815–4820.
[38] J. Liqiang, S. Xiaojun, C. Weimin, X. Zili, D. Yaoguo, F. Honggang, J. Phys. Chem. Solids. 64 (2003) 615–623.
[39] S.-J. Tsai, S. Cheng, Catal. Today. 33 (1997) 227–237.
[40] O. Pikuda, C. Garlisi, G. Scandura, G. Palmisano, J. Catal. 346 (2017) 109–116.
[41] H. Liu, W. Yang, Y. Ma, Y. Cao, J. Yao, New J. Chem. 26 (2002) 975–977.
[42] N. Arconada, Y. Castro, A. Durán, Appl. Catal. A 385 (2010) 101–107.
[43] J.G. Yu, J.C. Yu, Chin. J. Chem. 21 (2003) 994–997.
[44] J.G. Yu, J.C. Yu, W.K. Ho, Z.T. Jiang, New J. Chem. 26 (2002) 607–613.
[45] S. Li, G. Ye, G. Chen, J. Phys. Chem. C 113 (2009) 4031–4037.
[46] A.R. Liu, S.M. Wang, Y.R. Zhao, Z. Zheng, Mater. Chem. Phys. 99 (2006) 131–134.
[47] X. Chuan, Appl. Catal. B 51 (2004) 255–260.
[48] Y.V. Kolen'ko, B.R. Churagulov, M. Kunst, L. Mazerolles, C. Colbeau-Justin, Appl. Catal. B 54 (2004) 51–58.
[49] S. Dai, Y. Wu, T. Sakai, Z. Du, H. Sakai, M. Abe, Nanoscale Res. Lett. 5 (2010) 1829–1835.
[50] M. Andersson, L. Osterlund, S. Ljungstrom, A. palmqvist, J. Phys. Chem. B 106 (2002) 10674–10679.
[51] M. Wu, J. Long, A. Huang, Y. Luo, S. Feng, R. Xu, Langmuir 15 (1999) 8822–8825.
[52] J. Zhou, B. Song, G. Zhao, G. Han, Nanoscale Res. Lett. 7 (2012) 217–226.
[53] S.Y. Chae, M.K. Park, S.K. Lee, T.Y. Kim, S.K. Kim, W.I. Lee, Chem. Mater. 15 (2003) 3326–3331.
[54] Y. Ao, J. Xu, D. Fu, Appl. Surf. Sci. 256 (2009) 239–245.
[55] D.P. Serrano, G. Calleja, R. Sanz, P. Pizarro, Chem. Commun. 10 (2004) 1000–1001.
[56] S. Wang, L. Ji, B. Wu, Q. Gong, Y. Zhu, J. Liang, Appl. Surf. Sci. 255 (2008) 3263–3266.
[57] Z. Wang, D. Xia, G. Chen, T. Yang, Y. Chen, Mater. Chem. Phys. 111 (2008) 313–316.
[58] S.J. Kim, S. Park, Jpn. J. Appl. Phys. 40 (2001) 6797–6802.
[59] I.R. Ocaña, A. Beltram, J.J. Delgado Jaén, G. Adami, T. Montini, P. Fornasiero, Inorg. Chim. Acta. 431 (2015) 197–205.
[60] R. Kaplan, B. Erjavec, G. Dražić, J. Grdadolnik, A. Pintar, Appl. Catal. B 181 (2016) 465–474.
[61] M. Wu, G. Lin, D. Chen, G. Wang, D. He, S. Feng, R. Xu, Chem. Mater 14 (2002) 1974–1980.
[62] H. Yin, Y. Wada, T. Kitamura, S. Kambe, S. Murasawa, H. Mori, T. Sakata, S. Yanagida, J. Mater. Chem. 11 (2001) 1694–1703.
[63] M. Ousmane, L.F. Liotta, G. Di Carlo, G. Pantaleo, A.M. Venezia, G. Deganello, L. Retailleau, A. Boreave, A. Giroir-Fendler, Appl. Catal. B 101 (2011) 629–637.
[64] N. Bouazza, M. Ouzzine, M.A. Lillo-Ródenas, D. Eder, A. Linares-Solano, Appl. Catal. B 92 (2009) 377–383.
[65] Z. Bacsik, J. McGregor, J. Mink, Food Chem. Toxicol. 45 (2007) 266–271.
[66] F. Mühlberger, T. Streibel, J. Wieser, A. Ulrich, R. Zimmermann, Anal. Chem. 77 (2005) 7408–7414.
[67] A.K. Ghoshal, S.D. Manjare, J. Loss Prev. Process Ind. 15 (2002) 413–421.
[68] D. Cazorla-Amorós, J. Alcañiz-Monge, M.A. De la Casa-Lillo, A. Linares-Solano, Langmuir 14 (1998) 4589–4596.
[69] F. Rodriguez-Reinoso, A. Linares-Solano, Chem. Phys. Carbon 21 (1988) 1–146.
[70] H. Zhang, J.F. Banfield, J. Phys. Chem. B. 104 (2000) 3481–3487.
[71] A.R. Gandhe, J.B. Fernandes, J. Solid State Chem. 178 (2005) 2953–2957.
[72] R. López, R. Gómez, J. Sol-Gel Sci. Technol. 61 (2012) 1–7.
[73] M.A. Lillo-Ródenas, N. Bouazza, A. Berenguer Murcia, J. Linares Salinas, P. Soto, A. Linares Solano, Appl. Catal. B 71 (2007) 298–309.
[74] K.S.W. Sing, D.H. Everett, R.A.W. Haul, L. Moscou, L.A. Pierotti, J. Rouquerol, T. Siemieniewska, Pure Appl. Chem. 57 (1985) 603–619.
[75] T. Aguilar, J. Navas, R. Alcántara, C. Fernández-Lorenzo, J.J. Gallardo, G. Blanco, J. Martín-Calleja, Chem. Phys. Lett. 571 (2013) 49–53.
[76] A.A. Gribb, J.F. Banfield, Am. Mineral. 82 (1997) 717–728.
[77] M. Bellardita, A. Di Paola, B. Megna, L. Palmisano, Appl. Catal. B 201 (2017) 150–158.
[78] B. Ohtani, O.O. Prieto-Mahaney, D. Li, R. Abe, J. Photochem. Photobiol. A 216 (2010) 179–182.
[79] G. Marcì, E. García-López, M. Bellardita, F. Parisi, C. Colbeau-Justin, S. Sorgues, L.F. Liotta, L. Palmisano, Phys. Chem. Chem. Phys. 15 (2013) 13329–13342.
[80] Y. Hu, H. Tsai, C. Huang, J. Eur. Ceram. Soc. 23 (2003) 691–696.
[81] M. Janus, B. Tryba, E. Kusiak, T. Tsumura, M. Toyoda, M. Inagaki, A.W. Morawski, Catal. Lett. 128 (2009) 36–39.
[82] B. Tryba, M. Tygielska, J. Orlikowski, J. Przepiórski, React. Kinet. Mech. Catal. 119 (2016) 349–365.
[83] M.D. Hernández-Alonso, S. García-Rodríguez, S. Suárez, R. Portela, B. Sánchez, J.M. Coronado, Catal. Today 206 (2013) 32–39.
[84] R.J. Lobo-Lapidus, B.C. Gates, Chem. Eur. J. 16 (2010) 11386–11398.
[85] S. Doeuff, M. Henry, C. Sanchez, J. Livage, J. Non-Cryst. Solids 89 (1987) 206–216.
[86] F. Liu, X. Yan, X. Chen, L. Tian, Q. Xia, X. Chen, Catal. Today 264 (2016) 243–249.
[87] K.M. Glassford, J.R. Chelikowsky, Phys. Rev. B 46 (1992) 1284–1298.
[88] M.A. Lillo-Ródenas, N. Bouazza, A. Berenguer Murcia, J. Linares Salinas, P. Soto, A. Linares Solano, Appl. Catal. B 71 (2007) 298–309.
[89] M. Ouzzine, M.A. Lillo-Ródenas, A. Linares-Solano, Appl. Catal. B 134–135 (2013) 333–343.
[90] M. Nahar, J. Zhang, K. Hasegawa, S. Kagaya, S. Kuroda, Mater. Sci. Semicond. Process. 12 (2009) 168–174.
[91] J. Zhang, P. Zhou, J. Liu, J. Yu, Phys. Chem. Chem. Phys. 16 (2014) 20382–20386.